35th Annual International Conference of the IEEE EMBS
Osaka, Japan, 3 - 7 July, 2013

Threshold Choices of Huber Regularization Using Global- and Local-Edge-Detecting Operators for X-ray Computed Tomographic Reconstruction

Hua Zhang, Shanli Zhang, Debin Hu, Dong Zeng, Zhaoying Bian, Lijun Lu, Jianhua Ma, and Jing Huang*

***Abstract*— Statistical iterative reconstruction (SIR) approaches have shown great potential in x-ray computed tomographic (CT) reconstruction in the case of low-dose protocol. For yielding high quality image, an edge-preserving regularization should be incorporated into the objective function of SIR approaches. A typical example is the Huber regularization with an edge-preserving non-quadratic potential function which increases less rapidly than the quadratic potential function for sufficiently large arguments. However, a major drawback of the Huber regularization is the determining the threshold, which precludes its extensive applications. In this paper, we investigate both global- and local- edge-detecting operators for threshold choices of Huber regularization and apply them to SIR CT image reconstruction with low-dose scan protocol. Experiments were performed on XCAT phantom by using a CT simulator to obtain the low-dose projection data.**

I. Introduction

Due to the extensive applications of X-ray computed tomography (CT) in clinic, the associative radiation exposure from CT scans has raised major concerns to patients [1]. Cutting down the radiation exposure becomes one of the major efforts in the CT fields [2]. As a simple and cost-effective way, lowering the X-ray tube current and/or shortening the exposure time (mAs) in CT scan are easily realized to reduce radiation exposure. However, the associative image would suffer from serious noise and artifacts if without adequate noise treatments during image reconstruction. To solve above problem, statistical iterative reconstruction (SIR) approaches [3] as comparison with the filtered back-projection (FBP) approach, by incorporating the statistical properties of the measurement, have shown great potential to reduce the noise induced artifacts [3-5].

Under the assumption of Poisson statistic of CT projection measurement, the SIR approaches can be derived with the maximum a posteriori (MAP) estimator as given the measurement. The associative objective function of SIR usually consists two terms, i.e., 'data-fidelity term' and 'regularization term'. The data-fidelity term models the statistical measurement and the regularization term penalizes the solution. Usually, the regularization term is designed as a shift-invariant function that penalizes the disparity between the pixel intensities in a local neighborhood. These regularizations/priors through smoothing both noise and edge details equally often tend to produce unfavorable over-smoothing effects [4]. Different to the smoothing regularizations, many edge-preserving regularizations/priors were proposed in the literature [6,7]. A typical example is the Huber regularization [8], which replaces the quadratic penalty function with a non-quadratic penalty function that increases less rapidly than the quadratic penalty function for sufficiently large arguments.

One major drawback of the Huber function is the choice of the threshold. Many literatures have discussed it [9-11]. For example, Rousseeuw exploited the robust statistics approach to detect the outliers, and then presented a global edge-detecting operator for threshold choice [9]. Furthermore, using local statistical properties of the image, Black and Sapiro presented a local edge-detecting operator for threshold choice [10]. He et al defined a proportion variable, using discrete smoothing norm by Laplacian kernel, to restrict the threshold [11]. In summarizes, these techniques are all with the assumption that edges of the desired-image are not changing in generating the observation of image.

Due to the well expression of Huber regularization, it has been widely used in CT image reconstruction [12]. In this paper, we aim to investigate both global- and local- edge-detecting operators for threshold choices of Huber regularization [9,10] and apply them to SIR CT image reconstruction with low-dose scan protocol.

II. Materials and Methods

A. Penalized Weighted Least-Squares Image Reconstruction

Mathematically, the X-ray CT measurement can be approximately expressed as a discrete linear system:

$$y = \mathrm{H}\mu \tag{1}$$

where μ denotes the vector of attenuation coefficients, $i.e.,\ \mu = (\mu_1, \mu_2, ..., \mu_N)^T$ and y represents the obtained sinogram data (projections after system calibration and logarithm transformation), $i.e.,\ y = (y_1, y_2, ..., y_M)^T$, where '$T$' denotes the matrix transpose. The operator H represents the system or projection matrix with the size of $M \times N$. The element of H_{ij} denotes the length of intersection of projection ray i with pixel j. In the implementation, the associated element was pre-calculated by a fast ray-tracing

This work was supported in part by the NSF of China under Grants (Nos. 81101046 and 81000613), the Science and Technology Program of Guangdong Province of China under grant (No. 2011A030300005), and the 973 program of China under Grant (No. 2010CB732503). J. Ma also were supported in part by the National Key Technology Research and Development Program of the Ministry of Science and Technology of China under grant (No. 2011BAI12B03). National Science and Technology Major Project of the Ministry of Science and Technology of China (No. 2011YQ03011404). *Asterisk indicates corresponding author.*

H. Zhang, S. Zhang, D. Hu, Z. Zeng, Z. Bian, L. Lu, and J. Ma are with the School of Biomedical Engineering, Southern Medical University, Guangzhou 510515 China.

*J. Huang is with the School of Biomedical Engineering the Southern Medical University, Guangzhou 510515 China (telephone: 020-616-48285; e-mail: hjing@smu.edu.cn).

technique and stored as a file. The goal for CT image reconstruction is to estimate the attenuation coefficients μ from the measurement y.

According to the measurement model (1) and the MAP estimation criterion, the mathematical formula for PWLS image reconstruction with a regularization term $R(\mu)$ can be expressed as follows:

$$\mu^* = \arg\min_{\mu \geq 0} \left\{ (y - \mathrm{H}\mu)' \Sigma^{-1} (y - \mathrm{H}\mu) + \beta R(\mu) \right\} \quad (2)$$

where Σ is a diagonal matrix with the ith element of σ_i^2 which is the variance of sinogram data y. β is a hyper-parameter for controlling the strength of regularization

For determining the parameter σ_i^2 in equation (2), several methods can be used [4,13]. In this study, the variance of σ_i^2 was determined by the following mean-variance relationship proposed by Ma *et al* [13] recently:

$$\sigma_i^2 = \frac{1}{I_0} \exp(\bar{p}_i) \left(1 + \frac{1}{I_0} \exp(\bar{p}_i)(\sigma_e^2 - 1.25) \right) \quad (3)$$

where I_0 denotes the incident X-ray intensity, $\bar{p}_i$ is the mean of the sinogram data at bin i and σ_e^2 is the background electronic noise variance.

B. Huber Regularization

Traditionally, $R(\mu)$ in (2) is designed by a weighted sum of potential function about the disparity of neighboring pixels in image domain [4], which can be described as follows:

$$R(\mu) = \sum_j R(\mu_j) = \sum_j \sum_{k \in S_j} w(k,j) \varphi(\mu_j - \mu_k) \quad (4)$$

where index j runs over all image elements in the image domain. S_j represents a local neighborhood of the jth image pixel in two dimensions. The weight $w(k,j)$ is positive and symmetric, i.e., $w(k,j) \geq 0$ and $w(k,j) = w(j,k)$, which are usually designed to be an inverse proportion of the distance between pixels k and j in S_j. The φ denotes a convex and positive potential function satisfying $\varphi(0) = 0$.

There are many different choices of $\varphi(t)$. In this study, we investigate the Huber function φ_{Huber} defined as follows:

$$\varphi_{\mathrm{Huber}}(t) = \begin{cases} t^2/2, & |t| \leq \delta \\ \delta|t| - \delta^2/2, & |t| > \delta \end{cases} \quad (5)$$

The Huber potential function penalizes the disparity between neighboring pixels. As illustrated in Fig. 1, for $|t| < \delta$, the quadratic term produces a least-square fit for the image, and if $|t| > \delta$, a linearly varying cost is used which preserves the discontinuities of the image such as the edges.

In summary, the objective function of PWLS with the present Huber regularization (*i.e.*, PWLS-Huber) for CT image reconstruction can be rewritten as:

$$\mu^* = \arg\min_{\mu \geq 0} \left\{ (y - \mathrm{H}\mu)' \Sigma^{-1} (y - \mathrm{H}\mu) + \beta R_{\mathrm{Huber}}(\mu) \right\} \quad (6)$$

where the Huber regularization is defined as follows

$$R_{\mathrm{Huber}}(\mu) = \sum_j \sum_{k \in S_j} w(k,j) \varphi_{\mathrm{Huber}}(\mu_j - \mu_k). \quad (7)$$

In the implementation, a modified conjugate gradient (CG) method was adopted to optimize the objective function (6).

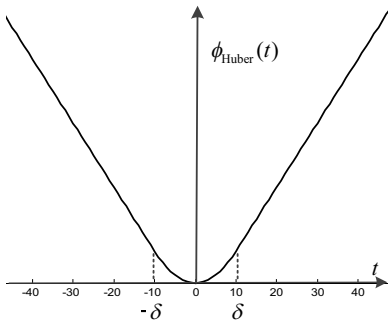

Fig. 1. An illustration of Huber potential function.

C. Huber Threshold Choice Strategies

A major advantage of the Huber model is its ability to switch the penalty on discontinuities according to the disparity of intensities between current pixel and its neighbors. This ability is produced by the Huber threshold δ, which plays a crucial role in determining the behavior of the Huber regularization. In this study, we investigate both global and local edge detecting operators for threshold choices of Huber regularization described as follows:

1) Global edge detecting method: According to the robust statistics, pixels with large gradient magnitude are viewed as outliers. The gradient at which a point is treated as an outlier is dependent on the parameter δ. And then the main idea is that δ should characterize the variance of the image [9]. So the robust measure of the data variability δ can be determined automatically in the following way:

$$\begin{aligned} \delta_G &= 1.4826\mathrm{MAD}(\nabla \mathrm{I}) \\ &= 1.4826\mathrm{median}_I(\|\nabla I - \mathrm{median}_I(\|\nabla I\|)\|) \end{aligned} \quad (8)$$

where "MAD" represents the median absolute deviation and the constant is originated from the fact that the MAD of a zero-mean normal distribution with unit variance is $0.6745 = 1/1.4826$.

2) Local edge detecting method: This part address how this parameter δ can be determined automatically from the image data in such a way that edges correspond to statistical outliers with respect to local image gradients [10]. The main idea is that δ should characterize the variance of the data within a region. δ varies across the image and hence, edge information is dependent on local statistical properties of the image. The local image detecting method shares the same robust statistical theory with the global one. In particular, we consider computing a local scale $\delta_L(p,q)$, which is a function of spatial position, in $n \times n$ pixel patches at every location in the image:

$$\delta_L(p,q) = 1.4826\mathrm{MAD}_{-\frac{n}{2} < i,j < \frac{n}{2}}(\nabla I_{p+i,q+j}). \quad (9)$$

III. Experiment and Results

The XCAT phantom was used for experimental data acquisition. The phantom was modeled with non-uniform rational

B-Spline surface based on the collected data. Accompanied with the XCAT phantom, a CT simulator was also provided. The projection data of phantom was simulated with a CT simulator at two mAs levels, $i.e$, 23.2 mAs and 580 mAs. For each mAs level, the tube voltage was set to be 120 kVp, the time per gantry rotation is 1.0 s, the slice thickness is 3 mm. The system geometry represented a system with 1,800 mm source-to-detector distance, 1510.4 mm center-to-source distance, and 0.8448 mm detector pixels (672 radial bins). Reconstructions were onto 0.86 mm square pixels with image size of 512$\times$ 512.

The following metrics were utilized to evaluate the noise reduction of the image reconstructed from the low-dose projection data: (1) local signal to noise ratio (lSNR); and (2) relative root mean square error (rRMSE):

$$\text{lSNR} = \frac{\frac{1}{Q}\sum_{m=1}^{Q}\mu_m}{\sqrt{\frac{1}{Q}\sum_{m=1}^{Q}\left|\mu_m - \frac{1}{Q}\sum_{m=1}^{Q}\mu_m\right|^2}} \tag{10}$$

$$\text{rRMSE} = \sqrt{\frac{\sum_{m=1}^{Q}|\mu_m - \mu_{G,m}|^2}{\sum_{m=1}^{Q}|\mu_{G,m}|^2}} \tag{11}$$

where μ represents the reconstructed image from the low-dose data, and μ_G denotes a golden standard image. m is the pixel index in the region of interest (ROI), and Q is the number of pixels in the ROI. In this study, the golden standard image was the image reconstructed by the FBP method with hanning filter from the projection data acquired with 580 mAs and 120 kVp.

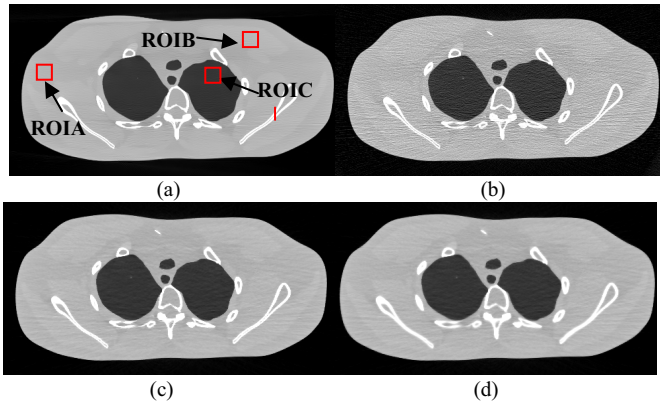

Fig. 2. XCAT phantom images reconstructed from the simulated projection data. (a) image reconstructed by the FBP method with optimal hanning filter from the projection data acquired with 580 mAs; (b) image reconstructed by the FBP method with ramp filter from the projection data acquired with 23.2 mAs; (c) image reconstructed by the PWLS-Huber algorithm with the global edge detecting method from the projection data acquired with 23.2 mAs ($\beta = 1.0 \times 10^3$); (d) image reconstructed by the PWLS-Huber algorithm with the local edge detecting method from the projection data acquired with 23.2 mAs ($n \times n$ =9 $\times$ 9, $\beta = 1.0 \times 10^3$). The display option is [0 0.03] mm^{-1}.

Fig. 2 shows the XCAT phantom images reconstructed from the simulated projection data. Fig. 2(a) is the image reconstructed by the FBP method with optimal hanning filter from the projection data acquired with 580 mAs. Fig. 2(b) is the image reconstructed by the FBP method with ramp filter from the projection data acquired with 23.2 mAs. Serious noise-induced streak artifacts can be observed compared with Fig. 2(a). Figs. 2(c)-(d) are the images reconstructed by the PWLS-Huber algorithm with the global edge detecting method and the local edge detecting method, respectively. It can be seen, with the two Huber threshold choice strategies, similar results were obtained with the noise and artifacts mostly suppressed. To further quantitatively evaluate the two Huber threshold choice strategies, the lSNR and rRMSE of three different ROIs, as indicated by the squares in Fig. 2(a), were measured as listed in Table 1. From the measuring results in Table 1, we can see the PWLS-Huber method with global and local edge detecting methods achieved much more gains than FBP, and the local edge detecting method performs better than the global edge detecting method in noise suppression in homogeneous regions. But from the profiles in Fig. 3, we can see that with the local edge detecting method, the reconstruction sacrifices more resolution than the global edge detecting method.

TABLE I

LSNR AND RRMSE MEASURES ON THE ROIS AS INDICATED BY THE SQUARES IN FIG. 2(A).

	ROI A		ROI B		ROI C	
Methods	lSNR	rRMSE	lSNR	rRMSE	lSNR	rRMSE
FBP	14.78	0.0674	12.90	0.0803	3.59	0.2761
PWLS-Huber(Global)	64.02	0.0187	66.78	0.0217	17.59	0.0683
PWLS-Huber(Local)	64.64	0.0186	67.48	0.0216	17.64	0.0680

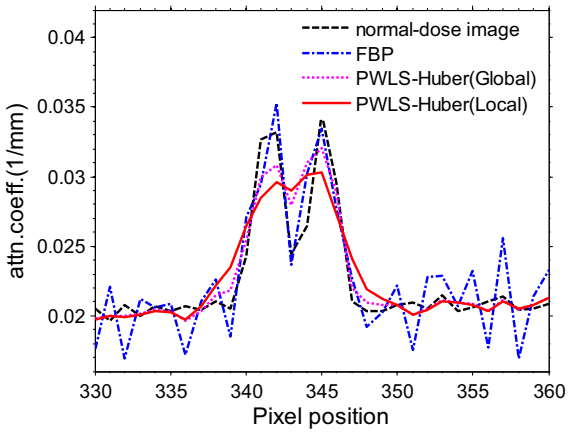

Fig. 3. Vertical profiles located at the pixel position x = 408 and y from 330 to 360 as indicated by the red line in Fig. 2(a).

For the global edge detecting method, the edge threshold δ in the Huber function is fixed once it has been calculated. But for the local edge detecting method, the parameter patch size ($n \times n$) can be varied. Fig. 4 shows the results of estimating

$\delta_L(p,q)$ in different pixel patches. Bright areas have higher values of $\delta_L(p,q)$ and correspond to more textured image regions. Fig. 5 shows the effects of the spatially varying $\delta_L(p,q)$. Moreover, Table 2 lists the measuring results of Figs. 5 in terms of lSNR and rRMSE. We can see that with the patch size changing from 5×5 to 17×17 the reconstructed image changed little. With patch size set to be 9×9, we may get a relative high-quality image.

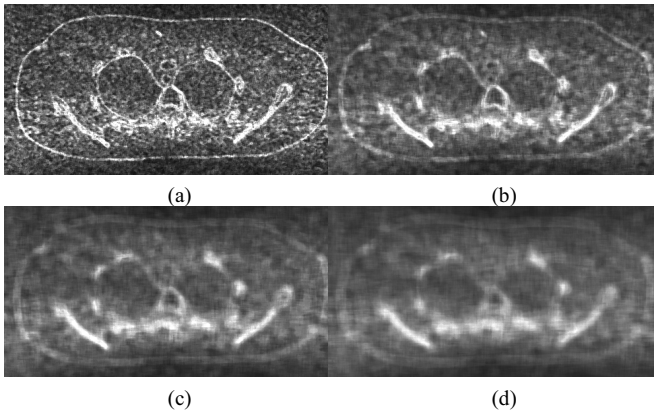

Fig. 4. Local estimate of scale $\delta_L(p,q)$. Bright areas correspond to larger values of $\delta_L(p,q)$. (a) $n \times n$ = 5 $\times$5; (b) $n \times n$ = 9 $\times$ 9; (c) $n \times n$ = 13 $\times$ 13; (d) $n \times n$ = 17 $\times$ 17.

TABLE II

lSNR AND rRMSE MEASURES ON THE ROIs (INDICATED BY THE SQUARES IN FIG. 2(A).) IN FIG. 5 WITH DIFFERENT LOCAL PATCH SIZE.

	ROI A		ROI B		ROI C	
Patch size	lSNR	rRMSE	lSNR	rRMSE	lSNR	rRMSE
5×5	64.90	0.0185	67.44	0.0216	17.61	0.0679
9×9	64.64	0.0186	67.48	0.0216	17.64	0.0680
13×13	64.32	0.0186	67.39	0.0217	17.63	0.0680
17×17	64.20	0.0186	67.31	0.0217	17.61	0.0681

IV. DISCUSSION AND CONCLUSION

In this paper, we investigate two state-of-the-art Huber threshold choice methods for CT statistical iterative reconstruction with low-dose scan protocol. Specifically, the global edge detecting method and the local edge detecting method were studied with the qualitative and quantitative measure. From the experimental result we can see that local edge detecting method performs more adaptively than the global edge detecting method as it introduced the local features of the desired image. But on the other hand, the local edge detecting method may sacrifice a little more image resolution than the global edge detecting method, which can be seen from smoothed edges.

One major limit of our study is the lack of clinic CT data validation, thus further study should be conducted on real patient data. Regarding to the other hyper-parameter β, it should also have influence on the quality of the final image. In this study, we just fixed it to only study the performance of different choice of the threshold δ, more quantitative experiments with considering both the two parameters should be performed.

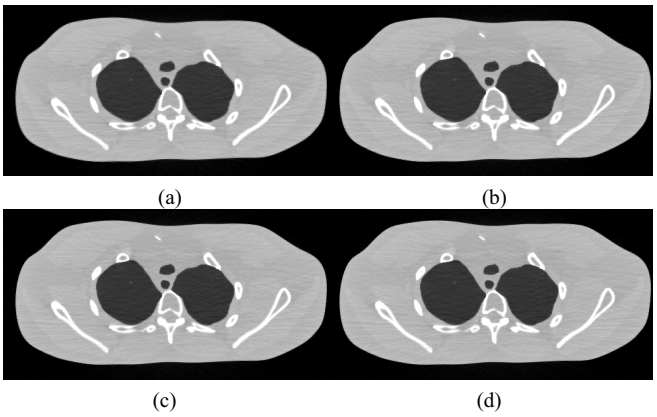

Fig. 5. Images reconstructed by the PWLS-Huber algorithm with the local edge detecting method of different patch size. (a) $n \times n$ = 5 $\times$5; (b) $n \times n$ = 9 $\times$ 9; (c) $n \times n$ = 13 $\times$ 13; (d) $n \times n$ = 17 $\times$ 17. The display option is [0 0.03] mm^{-1}.

REFERENCES

[1] D. J. Brenner, E. J. Hall, "Computed tomography–an increasing source of radiation exposure," *N Engl J Med Nov*, vol. 357, no. 22, pp. 2277-2284, 2007.

[2] J. Ma, J. Huang, Q. Feng, H. Zhang, H. Lu, Z. Liang, and W. Chen, "Low-dose computed tomography image restoration using previous normal-dose scan," *Med. Phys.*, vol. 38, pp. 5714-5731, 2011.

[3] S. Singh, M. K. Kalra, MD. Gilman, J. Hsieh, H. H. Pien, S. R. Digumarthy and J. A. Shepard, "Adaptive statistical iterative reconstruction technique for radiation dose reduction in chest CT: a pilot study," *Radiology*, vol. 259, no.2, pp. 565-573, 2011.

[4] J. Wang, T. Li, H. Lu, and Z. Liang, "Penalized weighted least-squares approach to sinogram noise reduction and image reconstruction for low-dose X-ray computed tomography," *IEEE Trans Med Imaging*, vol. 25, no. 10, pp. 1272-1283, 2006.

[5] J. Ma, H. Zhang, Y. Gao, J. Huang, Z. Liang, Q. Feng, and W. Chen, "Iterative image reconstruction for cerebral perfusion CT using a pre-contrast scan induced edge-preserving prior," *Phys Med Biol*, vol. 57, no. 22, pp.7519-7542, 2012.

[6] D. F. Yu and J. A. Fessler, "Edge-preserving tomographic reconstruction with nonlocal regularization," *IEEE Trans Med Imaging*, vol. 21, pp. 159-73, 2002.

[7] J. Idier, "Convex half-quadratic criteria and interacting auxiliary variables for image restoration," *IEEE Transactions on Image Processing*, vol. 10, no.7, pp. 1001-1009, 2001.

[8] D. Shulman and J Herve, "Regularization of discontinuous flow fields," *In Proc. Workshop on Visual Motion*, pp.81-86, 1989.

[9] P. J. Rousseeuw and A. M. Leroy, "Robust Regression and Outlier Detection," New York: Wiley, 1987.

[10] M. Black and G. Sapiro, "Edges as outliers: anisotropic smoothing using local image statistics," *Proc. Scale-Space Theories in Computer Vision*, pp. 259-70, 1999.

[11] H. He and L.P. Kondi, "Choice of Threshold of the Huber-Markov Prior in MAP-based Video Resolution Enhancement", *Conference on Electrical and Computer Engineering*,Vol.2,pp. 801-804,2004. 2004.

[12] J. Wang, T. Li, and L. Xing, "Iterative image reconstruction for CBCTusing edge-preserving prior," *Med Phys*, vol. 36, no. 1, pp. 252-260, 2009.

[13] J. Ma, Z. Liang, Y. Fan, Y. Liu, J. Huang, W. Chen, and H. Lu, "Variance analysis of x-ray CT sinograms in the presence of electronic noise background," *Med Phys*, vol. 39, no. 7, pp. 4051-4065, 2012.